Using Clinopyroxene Chemistry to Constrain Magma Plumbing System in a 1.2 Ga Andesitic to Shoshonitic Volcanic Arc, Barby Formation, Namibia

By Lauren Burden[1], Dr. Richard Hanson[1], Dr. Steven Singletary[2]

Texas Christian University[1] and University of North Carolina, Pembroke[2]

SciCom Let's Talk Science

Abstract

The 1.2 Ga Barby Formation located in SW Namibia is comprised of basaltic andesites and shoshonites from oblique subduction in a volcanic arc setting. Recent mapping and whole-rock geochemistry within the Barby Formation has been completed by previous TCU graduate students. Clinopyroxenes (CPX) from samples collected during these studies were analyzed using an Electron Microprobe (EMP) at Fayetteville State University, North Carolina. Data collected from CPX phenocrysts corresponds with previous findings that the samples can be divided into two groups. Group 1 samples show an enrichment in rare earth elements (REE) and light rare earth elements (LREE) Th, Zr, La/Yb, Nb, with a smaller Ti anomaly as compared to Group 2 (Lehman, 2019; Orhmundt, 2020). CPX phenocrysts within Group 1 have higher TiO2 wt% concentrations. Differences between the two groups are attributed to different source rock compositions and partial melting (Lehman, 2019; Orhmundt, 2020). Mineral compositions and cation ratios from EPMA data were also used to determine geothermobarometric conditions of the formation's magma plumbing system. Single-clinopyroxene thermometry and barometry equations from Wang et al. (2021) and Purtika (2008) were utilized in this study. Wang et al. (2021) calculations resulted with average pressures between 1-3 ± 1.5 kbar and average temperatures between 1100-1200 °C. Purtika (2008) calculations resulted with overall higher pressures averaging at 3-5 kbar and slightly hotter temperatures at 1200 ± 50°C. Overall temperatures are higher than what would be expected in the basaltic andesitic system and variations could be due to the low-grade metamorphism the area has experienced that has affected the geochemistry.

Introduction and Statement of the Problem

The Barby Formation is a major rock unit within the Mesoproterozoic Konkiep terrane in southwest Namibia, which makes up part of the Namaqua-Natal orogenic belt (NNOB) in southern Africa (Figures 1 and 2). The formation consists mainly of calc-alkaline to shoshonitic basaltic andesites to andesites formed in a 1.2 Ga volcanic arc (Hoal, 1990; Miller, 2008). Here I use clinopyroxene (cpx) chemistry in Barby Formation rocks to help constrain magma chamber evolution and characterize the complex magma plumbing system. This study uses an electron microprobe to analyze cpx in previously samples collected by Andrews et al., (2016, 2017) (Figures 3 and 4) and Ohrmundt (2020) (Figures 5 and 6) to examine compositional trends and to constrain the magma source chamber characteristics through geothermobarometry.

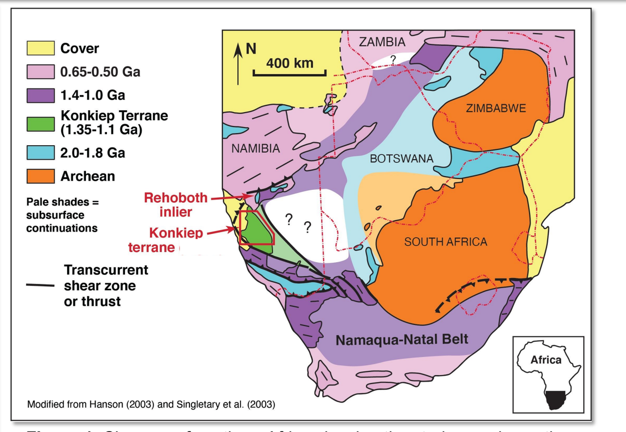

Figure 1. Close up of southern Africa showing the study area in southern Namibia. Modified from Hanson (2003) and Singletary et al. (2003).

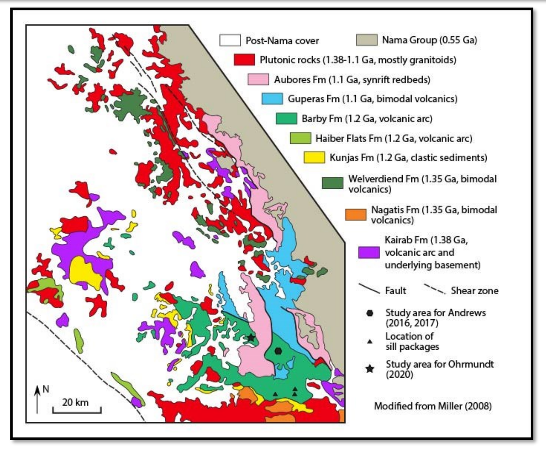

Figure 2. Geologic map of the Konkiep terrane in Figure 1 modified from Miller (2008). Field areas from previous TCU studies are indicated within the Barby Formation. Rocks collected from these sites are the focus of this study.

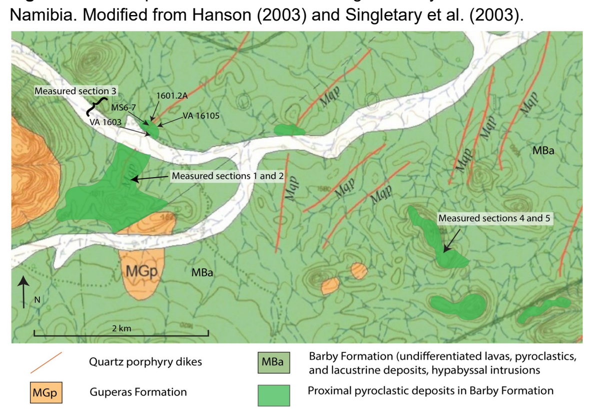

Figure 3. Map of Andrews et al. (2016) field area to the east of the Aubures half graben. Base map is from Watters (1974); imagery is downloaded from Google Earth (2022).

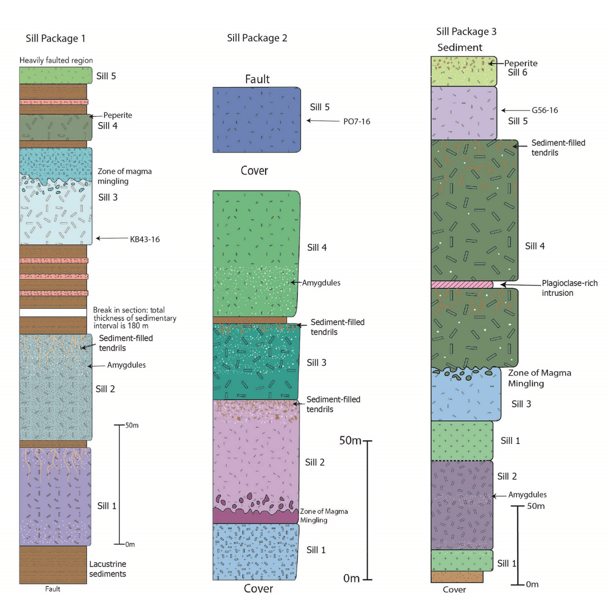

Figure 4 (above). Measured sections of sill packages 1-3 in Figure 3 (Andrews and Hanson unpublished data), showing location of samples analyzed in the present study. Brown color represents lacustrine sediment.

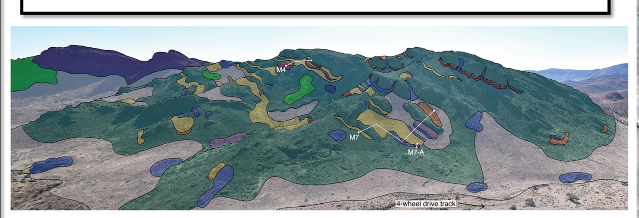

Figure 5. Oblique view of Ohrmundt's (2020) field area. Legend is the same as in Figure 5. Photo taken from west edge of the map in Figure 5 looking northeast from point A. Labels in photo represent locations of measured sections done by Ohrmundt (2020) and do not pertain to this project.

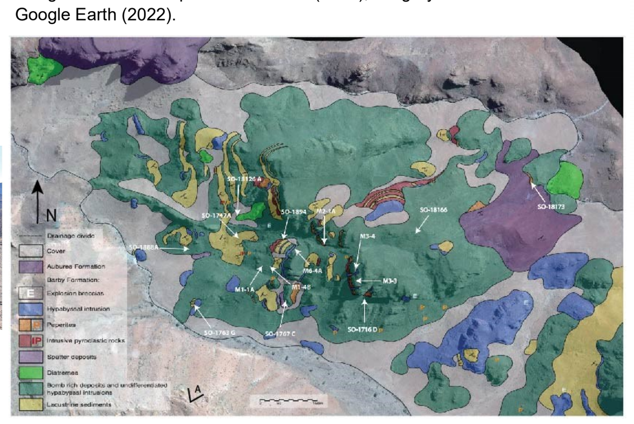

Figure 6 (left). Map modified from Ohrmundt (2020) of the Barby Formation in a well exposed area to the west of the Aubures half graben (Figure 2). White arrows indicate locations of samples analyzed in this study. A= location of panoramic photo shown in Figure 5.

Whole-rock Chemistry

Harker variation diagrams indicate a decrease in MgO and FeO with increasing silica content (Figures 7 and 8) (Lehman, 2019 and Ohrmundt, 2020). This is consistent with fractionating phenocrysts of olivine and cpx in the samples. Whole-rock compositions plot closely together as calc-alkaline basaltic andesites (Figures 9-11). All samples plot within the subalkaline field based on trace element data (Figure 9). However, sill samples plot slightly higher towards felsic compositions than other samples, but it is not enough to make a difference in the overall chemical composition. Figure 10 shows samples clustering tightly together in the calc-alkaline field. Figure 11 shows that the samples cluster on the border between calc-alkaline to shoshonitic basalts with the majority of the samples being more shoshonitic in composition.

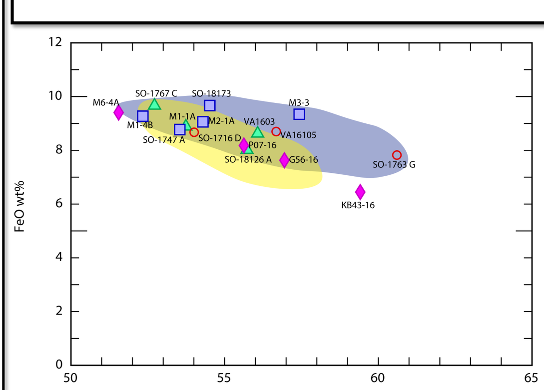

Figure 7. Harker variation diagram for FeO. Blue field represents samples from Ohrmundt (2020) and yellow field represents samples from Lehman (2019).

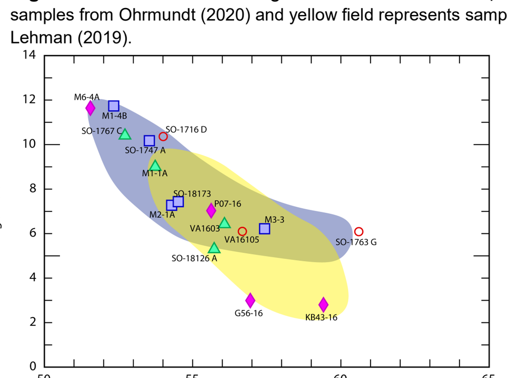

Figure 8 (left). Harker variation diagram of MgO. See Figure 7 for explanation of fields.

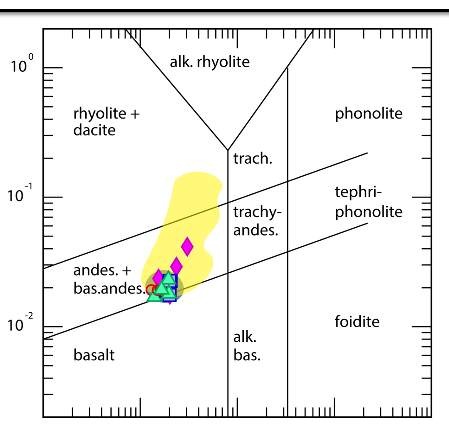

Figure 9 (left). Nb/Yb vs. Zr/Ti classification diagram from Pearce (1996). Alk. Rhyolite: alkali rhyolite; trach.: trachyte; trachyandes.: trachyandesite; andes. + bas. andes.: andesite + basaltic andesite; alk. bas.: alkali basalt. See Figure 7 for explanation of fields.

Legend
- Bomb
- Spatter and Agglutinate
- Sill
- Other Hypabyssal Intrusion
- Bedded Lapillistone

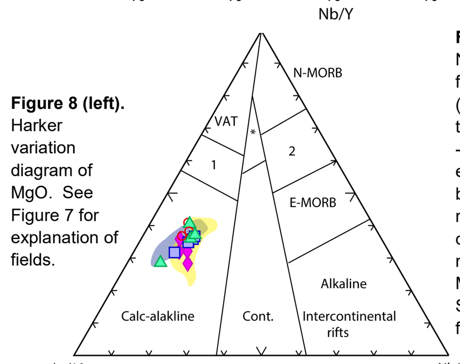

Figure 10 (left). La/10-Y/15-Nb/8 discrimination diagram from Cabanis and Lecolle (1989). VAT: volcanic arc tholeiite; N-MORB: normal mid -ocean ridge basalt; E-MORB: enriched mid-ocean ridge basalt; Cont.: Continental; 1 represents overlap between calc-alkaline and VAT; 2 represents weakly enriched MORB; *: back arc basalts. See Figure 7 for explanation of fields.

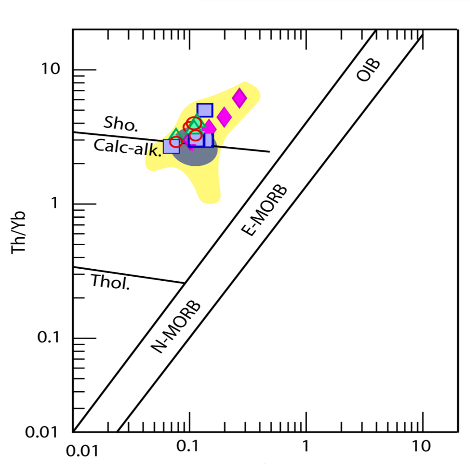

Figure 11. Ta/Yb vs. Th/Yb discrimination diagram from Pearce (1982). N -MORB: normal mid-ocean ridge basalt; E-MORB: enriched mid-ocean ridge basalt; OIB: ocean island basalt; Thol.: tholeiite; Calc-alk.: calc-alkaline; Sho.: shoshonite. See Figure 7 for explanation of fields.

Methodology

Petrographic studies using standard thin sections were used to visually estimate phenocryst and vesicle percentages and identify textures present in the minerals. Scanning electron microscope (SEM) images of cpx were taken to compare the textures seen with optical microscopy.

Geothermobarometry follows methods outlined by Putirka (2008) and Wang et al. (2021) using cpx-only thermobarometer. Both techniques were calibrated using experimental hydrous systems for mafic lavas. The Putirka (2008) has a standard error of estimate (SEE) of ±5 kbar and the SEE for the thermometer is ± 50-60 °C. The Wang et al. (2021) barometer has an SEE of ±1.66 kbar and the thermometer has an SEE equal to ±36.6 °C. The thermometer accounts for H_2O (wt%) solve for T. However, because rocks used in this study have been altered, H_2O is neglected for this study.

Cpx Chemistry Results

Petrographic analysis indicates that low-grade metamorphic and alteration products are abundant in every sample. Igneous disequilibrium textures characteristic of intermediate rocks are common. Oscillatory zoning in cpx can be seen in SEM imagery and under the petrographic microscope, indicating changes in magma chamber composition causing disequilibrium during crystal growth.

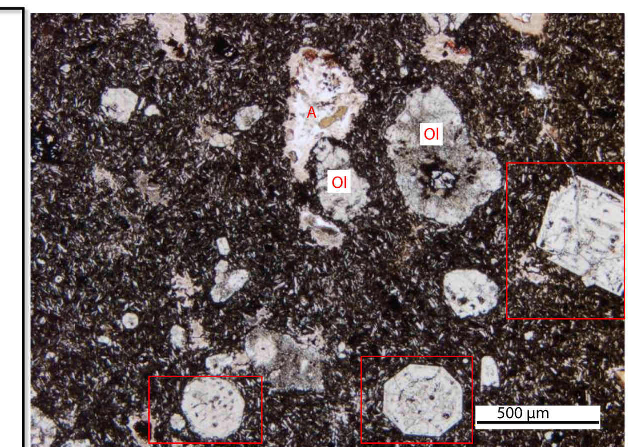

Figure. 12 Pyroclastic bomb sample SO-1747A with rectangles outlining cpx phenocrysts. Groundmass shows intersertal texture. A: amygdule; Ol: olivine.

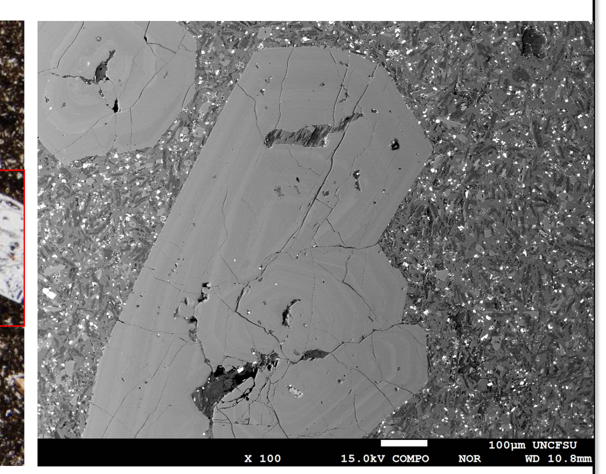

Figure 13. Hypabyssal intrusion sample SO-1894 showing cpx phenocrysts with excellent oscillatory zoning. The larger crystal in the center is a glomerocryst. White scale bar (100 μm) is shown at the bottom of the image.

Ohrmundt data are tightly clustered in the diopside and augite field. Diopside is generally more abundant in these samples (Figure 14). Andrews data are also tightly clustered in the diopside and augite field, but the samples are generally more abundant in augite, including some subcalcic augite in sample KB43-16 (Figure 15). Variations in average values for major oxides FeO, MnO, and Cr_2O_3 as well as for Mg# are shown in Figures 16-18. All samples show a strong trend for decreasing FeO with increasing Mg# (Figure 16). In contrast, Cr_2O_3 increases with Mg# (Figure 17), which is expected because Cr is compatible in cpx (Deer et al., 2013). Generally, samples show increasing FeO with decreasing MnO (Figure 18). All three of these inclinations are typical trends in cpx (Deer et al., 2013). Cpx phenocrysts in sill packages 1-3 in Andrews' study (PO7-16, G56-16, and KB43-16) area show unusual trends as compared to the rest of the samples, with higher total FeO and MnO, low Cr_2O_3 , and low Mg# (Figures 16-18). Sample VA 16105, a hypabyssal intrusion, also tends to plot away from the main trend and closer to the sill package samples.

Legend
- Bomb
- Spatter and Agglutinate
- Sill
- Other Hypabyssal Intrusion
- Bedded Lapillistone

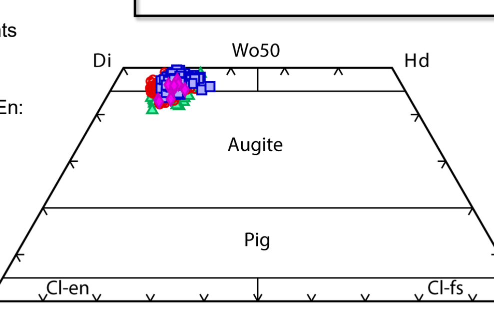

Figure 14. All data points for cpx analyzed from samples collected from Ohrmundt's field area. En: enstatite; Cl-en: clinoenstatite; Fs: ferrosilite; Cl-fs: clinoferrosilite; Pig: pigeonite; Di: diopside; Wo: Wollastonite; Hd: hedenbergite.

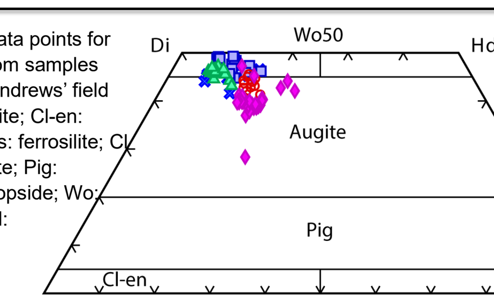

Figure 15. All data points for cpx analyzed from samples collected from Andrews' field area. En: enstatite; Cl-en: clinoenstatite; Fs: ferrosilite; Cl-fs: clinoferrosilite; Pig: pigeonite; Di: diopside; Wo: Wollastonite; Hd: hedenbergite.

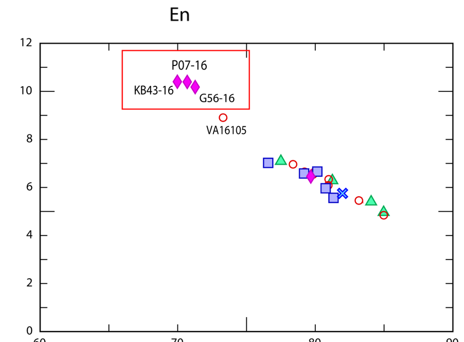

Figure 16. Average Mg# vs. FeO wt% for individual crystals. Red box indicates samples from sill packages.

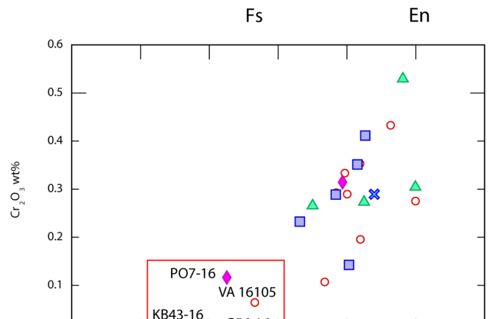

Figure 17. Average Mg# vs. Cr_2O_3 wt% for individual crystals. Red box indicates sill packages and one other hypabyssal intrusion.

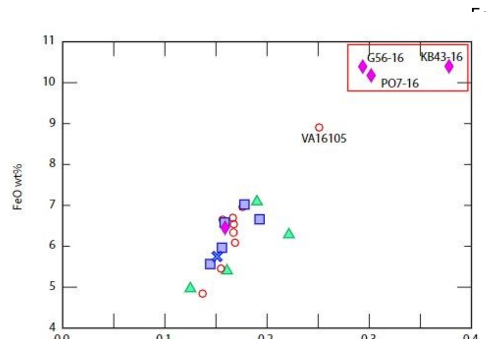

Figure 18. Average FeO vs. MnO wt% for individual crystals. Red box indicates samples from sill packages.

Temperature and Pressure Results

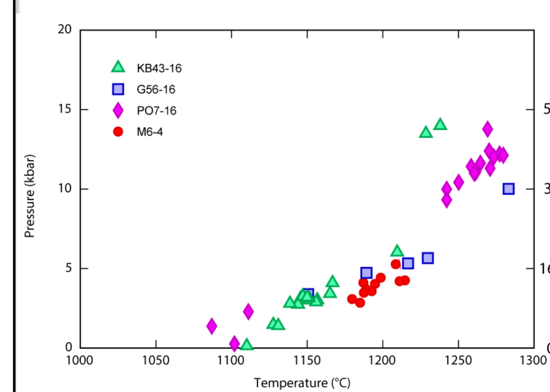

Figure 19. Temperature and pressure results for sills.

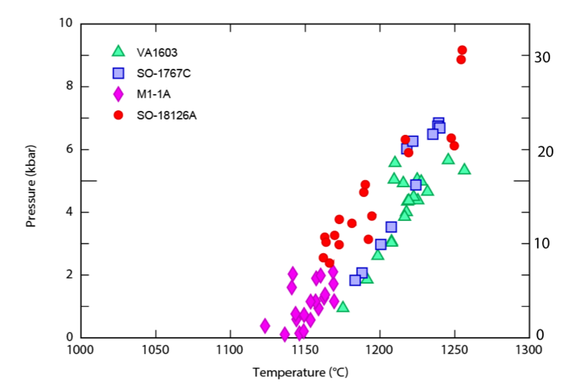

Figure 20. Temperature and pressure results for spatter and agglutinate.

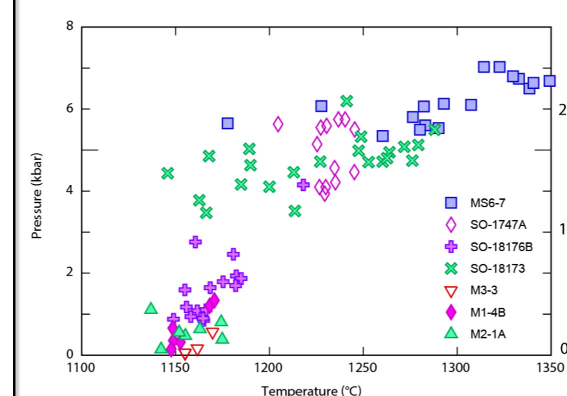

Figure 21. Temperature and pressure results for pyroclastic bombs.

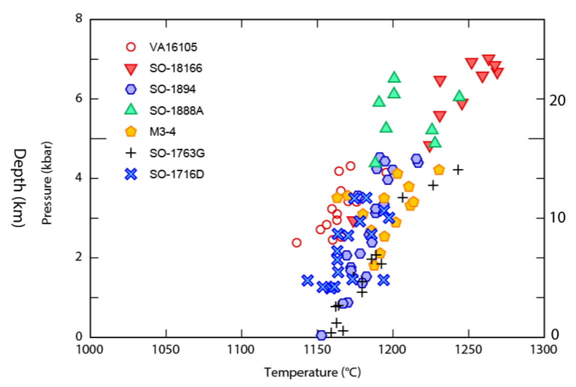

Figure 22. Temperature and pressure results for other hypabyssal intrusions.

Average temperature values range from ~1150-1300 °C . Average pressure values range from ~0-10 kbar. Some data points from cpx in hypabyssal intrusions and bomb samples with higher TiO_2 yielded negative pressures due to a lower Al^{VI} content. These data points were omitted from Figures 22 and 23. The wider range between temperatures using this calibration is likely due to magma mixing during cpx crystallization. Sill package samples with extremely high pressures result in depths up to ~46 km. These pressures should be treated with great caution due to their wide range from the same samples. Most cpx samples within the data set show a downward trend from 6-7 kbar for pyroclastic bombs, agglutinate, and hypabyssal intrusions. This trend could be consistent with magma staging in the mid-crust seen in volcanic arc settings (Rosell et al., 2015). However, the downward trend on calculated pressures also indicates issues and suggests alteration or disequilibrium effects.

Results from Wang et al. (2021) are highlighted over Putirka (2008) due to the lower SEE for both pressures and temperatures. However, both techniques calculated inconsistent or negative pressures. Part of the problem with inconsistent pressures could be that the Wang et al. (2021) barometer is only calibrated for pressures up to 12 kbar, meaning that the cpx in some of my samples might have crystallized out of the calibration range for the barometer. Overall, Wang et al. (2021) calibrations give temperatures consistent with basaltic andesites (e.g. Sheehan and Barclay, 2016; Feng and Zhu, 2019).

Conclusions

- Based on cpx and whole-rock chemistry, majority of the samples experienced the same petrogenetic history.
- Exceptions to this include samples collected from sill packages 1, 2, and 3 and VA16105, a different hypabyssal intrusion. Cpx chemistry from these samples indicate a different petrogenetic history than the other samples.
- Geothermobarometric results indicate temperatures from most samples that are expected from an andesitic to shoshonitic system, ~1150-1250 °C (e.g. Sheehan and Barclay, 2016; Feng and Zhu, 2019). Resultant pressures should be treated with caution due to the wide range calculated.
- Most samples indicate the highest pressures at ~6-7 kbar. This could indicate magma storage beginning in the middle crust, ~8-15 km deep (Rossel et al., 2015).

References

Andrews, V.P., Hanson, R.E., Baylor, D., Lehman, K.M., and Williams, J.W, 2016, Intermixed hawaiian, strombolian, and phreatomagmatic eruption styles in a Mesoproterozoic volcanic arc sequence (Barby Formation) in southwest Namibia: Geological Society of America Abstracts with Programs, v. 48, no. 7, doi: 10.1130/abs/2016AM-283694.

Andrews, V.P., Hanson, R.E., Lehman, K.M., Baylor, D., and Williams, J.W., 2017, Volcanic and hypabyssal lithofacies in a Mesoproterozoic volcanic arc sequence, Barby Formation, southwest Namibia: Geological Society of America Abstracts with Programs, v. 49, no. 1, doi: 10.1130/abs/2017SC-289494.

Cabanis, B., and Lecolle, M., 1989, The La/10-Y/15-Nb/8 diagram: a tool for discriminating volcanic series and evidencing continental crust magmatic mixtures and/or contamination: Comptes rendus de l'Academie des sciences, Serie 2, Mecanique, Physique, Chimie: Sciences de l'univers, Sciences de la Terre, v. 309, p. 2023-2029.

Deer, W.A., Howie, R.A., and Zussman, J., 2013, An Introduction to Rock Forming Minerals: London, Mineralogical Society of Great Britain and Ireland, 3rd edition, 498 p.

Feng, W. and Zhu, Y., 2019, Magmatic plumbing system beneath a fossil continental arc volcano in western Tianshan (nw China): constraints from clinopyroxene and thermodynamic modeling: Lithos, v. 350-351, 20 p. doi: 10.1016/j.lithos.2019.105221.

Hanson, R.E., 2003, Proterozoic geochronology and tectonic evolution of southern Africa, *in* Yoshida, M., Windley, B., and Dasgupta, S., eds., Proterozoic East Gondwana: Supercontinent Assembly and Breakup: Geological Society of London Special Publication 206, p. 428-463.

Hoal, B.G., 1990, The geology and geochemistry of the Proterozoic Awasib Mountain Terrain, southern Namibia: Geological Survey of Namibia, Memoir 11, 163 p.

Lehman, K.M., 2019, Exploring the geochemical evolution of magmatic sources in relation to tectonic setting in the Mesoproterozoic Konkiep terrane, Namaqua-Natal orogen, SW Namibia [M.S. Thesis]: Texas Christian University, 243 p.

Miller, R. McG., 2008, The Geology of Namibia, Vol. 1, Archaean to Mesoproterozoic: Windhoek, Geological Survey of Namibia, p. 8-1 to 8-104.

Ohrmundt, S.C., 2020, Eruptive styles, magma-plumbing systems, and magma/sediment interaction in a 1.2 Ga calc-alkaline to shoshonitic volcanic arc setting, SW Namibia [M.S. Thesis]: Texas Christian University, 75 p.

Pearce, J.A., 1996, A users guide to basalt discrimination diagrams, *in* Bailes, A.H. Christiansen, E.H., Galley, A.G., Jenner, G.A., Keith, Jeffrey D., Kerrich, R., Lentz, David R., Lesher, C.M., Lucas, Stephen B., Ludden, J.N., Pearce, J.A., Peloquin, S.A., Stern, R.A., Stone, W. E., Syme, E.C., Swinden, and H.S., Wyman, D.A., eds., Trace element geochemistry of volcanic rocks; applications for massive sulphide exploration, Geological Association of Canada, Short Course Notes, v. 12, p. 79-113.

Putirka, K.D., 2008, Thermometers and barometers for volcanic systems: Reviews in Mineralogy and Geochemistry, vol. 69, p. 66-120.

Rossel, P., Oliveros, V., Ducea, M.N., and Hernandez, L., 2015, Across and along arc geochemical variations in altered volcanic rocks: Evidence from mineral chemistry of Jurassic lavas in northern Chile, and tectonic implications: Lithos, v. 239, p. 97-113.

Sheenhan, F. and Barclay, J., 2016, Staged storage and magma convection at Ambryn volcano, Vanuatu, Journal of Volcanology and Geothermal Research 322, p. 144-157.

Singletary, S.J., Hanson, R.E., Martin, M.W., Crowley, J.L., Bowring, S.A., Key, R.M., Ramokate, L.V., Direng, B.B., and Krol, M.A., 2003, Geochronology of basement rocks in the Kalahari Desert, Botswana, and implications for regional Proterozoic tectonics: Precambrian Research, v. 121, p. 47-71.

Wang, X., Hou, T., Wang, M., Zhang, C., Zhang, Z., Pan, R., Marxer, F., and Zhang, H., 2021, A new clinopyroxene thermobarometer for mafic to intermediate magmatic systems: European Journal of Mineralogy, v. 33, p. 621-637.

Watters, B.R., 1974, Stratigraphy, igneous petrology and evolution of the Sinclair Group in southern South West Africa: Bulletin of the Precambrian Research Unit, University of Cape Town, v. 16, 235 p.